Enhancement of the Catalytic Activity Associated with Carbon Deposition Formed on NiO/Al_2O_3 During the Dehydrogenation of Ethane and Propane

Shigeru SUGIYAMA[1]*, Akihiko KOIZUMI[1], Takahisa IWAKI[1], Naohiro SHIMODA[1], Yuki KATO[2], and Wataru NINOMIYA[2]

[1]*Department of Applied Chemistry, Tokushima University, Minamijosanjima, Tokushima-shi, Tokushima 770-8506, Japan*

[2]*Hiroshima R&D Center, Mitsubishi Chemical Corporation, 20-1, Miyuki-cho, Otake-shi, Hiroshima 739-0693, Japan*

Keywords: Dehydrogenation, Ethane, Propane, Nickel Oxide, Catalyst Deactivation

In the recent study, the dehydrogenation of isobutane to isobutene was accomplished using a $NiO/\gamma\text{-}Al_2O_3$ catalyst, and significant improvement in the time-on-stream yield of isobutene was accomplished. During the normal catalytic dehydrogenation of alkanes, the catalyst is covered by the carbon deposition that is generated during the reaction, which drastically reduces activity with time-on-stream. Therefore, no examples of the catalytic dehydrogenation of isobutane have yet been reported. This study used either ethane or propane as a source of isobutane to examine whether the activity was improved with time-on-stream. As a result, in the dehydrogenations of both ethane and propane on a $NiO/\gamma\text{-}Al_2O_3$ catalyst, the catalytic activity decreased with time-on-stream when the supporting amounts of NiO was small. By contrast, when the supporting amount of NiO was large, the catalytic activity improved with time-on-stream. The results using a $NiO/\gamma\text{-}Al_2O_3$ catalyst with small and large NiO loadings were similar to those of isobutane dehydrogenation and it was confirmed that the dehydrogenation activity was improved with time-on-stream in the catalytic dehydrogenations of ethane, propane, and isobutane using large NiO loadings. Intermediate behavior using a moderate amount of NiO loading, which was not detected in the dehydrogenation of isobutane, was also observed, which resulted in a maximum yield of either ethylene or propylene at 2.0 or 3.25 h on-stream, respectively. We concluded that the reason the catalytic activity did not improve with time-on-stream when using a $NiO/\gamma\text{-}Al_2O_3$ catalyst was because the supporting amount of NiO was too small. These results show that activity with time-on-stream could also be improved in the dehydrogenations of other alkanes.

Introduction

When using a solid catalyst, deactivation is a problematic phenomenon. When an organic chemical reaction is carried out on a solid catalyst, the surface of the solid catalyst is covered with the deposition of carbon by-product, which drastically reduces the catalytic activity (Argyle and Bartholomew, 2015).

In the case of catalytic oxidation, carbon deposition on the surface can be burned off by the vapor phase of oxygen and removed as carbon dioxide. Therefore, the catalyst deactivation due to carbon deposition is relatively small during catalytic oxidation. On the other hand, in the case of catalytic dehydrogenation, the amount of carbon deposition that covers the catalyst surface increases with time-on-stream. Therefore, catalyst deactivation due to carbon deposition is a fatal problem with catalytic dehydrogenation.

Despite this normal background, when dehydrogenation of isobutane to isobutene was performed in our laboratory using a $NiO/\gamma\text{-}Al_2O_3$ catalyst, we found that the isobutene yield was improved significantly with time-on-stream (Sugiyama *et al*., 2021). Since nickel oxide on the supported catalyst is reduced to metallic Ni at the initial stage of the reaction, the metallic nickel species becomes the active catalytic site. For a long time, it has generally been accepted that the use of metallic Ni as a catalyst will result in a significant reduction in catalytic activity with time-on-stream due to the remarkable formation of carbon deposits (Miura *et al.*, 1968). This occurs in various reactions: dehydrogenation (Ding *et al*., 2010a; Ye *et al*., 2019), steam reforming (Besenbacher *et al*., 1998; Sehested, 2006; Guo *et al*., 2007; Ochoa *et al*., 2017), methane decomposition (Otsuka and Takenaka, 2003; Avevalo *et al*., 2017), dry reforming (Bradford and Vannice, 1999; Hayakawa *et al*., 1999; Arora and Prasad, 2016), and partial oxidation reactions (Takehira *et al*., 2002; Alvarez-Galvan *et al*., 2019). Therefore, the dehydrogenation of isobutane on $NiO/\gamma\text{-}Al_2O_3$ in the previous study achieved results contrary to conventional wisdom. Based on these results, we were compelled to address the following questions.

1. Could this phenomenon be anomalous only to the catalytic dehydrogenation of isobutane?
2. Although $NiO/\gamma\text{-}Al_2O_3$ is often used for catalytic dehydrogenation, we wondered why there was no such improvement in the yield of the target product with time-on-stream.

Received on March 24, 2022, Accepted on July 2, 2022

DOI:10.1252/jcej.22we028

Correspondence concerning this article should be addressed to S. Sugiyama (E-mail address: sugiyama@tokushima-u.ac.jp)

To elucidate these points, in the present study, we investigated the dehydrogenation of ethane to ethylene and propane to propylene on a NiO/γ-Al_2O_3 catalyst. In the present study, the key reactions of dehydrogenation and carbon depositions are represented by equations (1) and (2), respectively.

$C_xH_{2x+2} \rightarrow C_xH_{2x} + H_2$ (x= 2 or 3) (Eq. 1)
$C_xH_{2x+2} \rightarrow xC + (x+1)H_2$ (x = 2 or 3) (Eq. 2)

1. Experimental Section

1.1 Preparation of the catalysts

The catalyst referred to as NiO(x)/γ-Al_2O_3, in which "x" indicates the content by weight %, defined as 100 × NiO [g] / (γ-Al_2O_3 [g] + NiO [g]), was prepared via the impregnation method, as previously reported (Ding *et al*., 2010a; Sugiyama *et al*., 2021). As an example of the catalyst preparation, the method used to prepare NiO(5)/γ-Al_2O_3 is as follows. Into 30 mL of an aqueous solution containing 0.819 g of dissolved $Ni(NO_3)_2{\cdot}6H_2O$ (Fujifilm Wako Pure Chemical Co.), 4.000 g of γ-Al_2O_3 (JRC-ALO-9, which served as a reference catalyst from the Catalysis Society of Japan) was added. The suspension was then evaporated via drying at 383 K for 12 h. Finally, the resultant solid was calcined at 823 K.

1.2 Characterization of catalysts

The specific surface area, total pore volume, and average pore diameter were estimated using the nitrogen adsorption isotherms of the catalysts pretreated at 473 K for 5 h using a BELSORPmax12 (MicrotracBEL) at 77 K. X-ray diffraction (XRD) patterns were measured using a SmartLab/R/INP/DX (Rigaku Co.) with a Cu Kα radiation monochromator at 45 kV and 150 mA. Thermogravimetric analysis was carried out using a EXSTAR6000 (Seiko Instruments Inc.) under 100 mL/min of air flow at a heating rate of 8 K/min from 298 to 1073 K. Raman spectroscopy was measured via an inVia Reflex (Renishaw K. K.). Some catalysts were observed using field emission scanning electron microscopy (FE-SEM) using a JSM-7400F (JEOL Ltd.).

1.3 Evaluation of catalytic performances

A fixed-bed continuous-flow reactor operated under atmospheric pressure was used for the activity test on each of the catalysts (0.25 g), which were previously pelletized and sieved to reach a size of 1.18–1.70 mm, at 823 or 923 K for the dehydrogenation of propane or ethane, respectively. The temperature of the catalyst was increased to the reaction temperature under a He flow. After the reaction temperature was stabilized, tests were carried out under a reactant gas that consisted of $P(C_2H_6$ or $C_3H_8)$ = 14.1 kPa and P(He) = 87.2 kPa at a flow rate of 15.0 mL/min. The homogeneous reactions were negligible under these conditions for both dehydrogenations. The reaction behavior was analyzed using a gas chromatograph (GC-8APT, Shimadzu Corp.) equipped with a thermal conductivity detector (TCD). The columns in the TCD-GC consisted of the following: a molecular sieve (5A) (0.3 m×Φ3 mm) for the detection of CO and CH_4, and a Porapak Q (6 m×Φ 3 mm) for the detection of C_2H_4, C_2H_6, C_3H_6, and C_3H_8. The conversion of ethane and propane (C_{C2H6} and C_{C3H8},

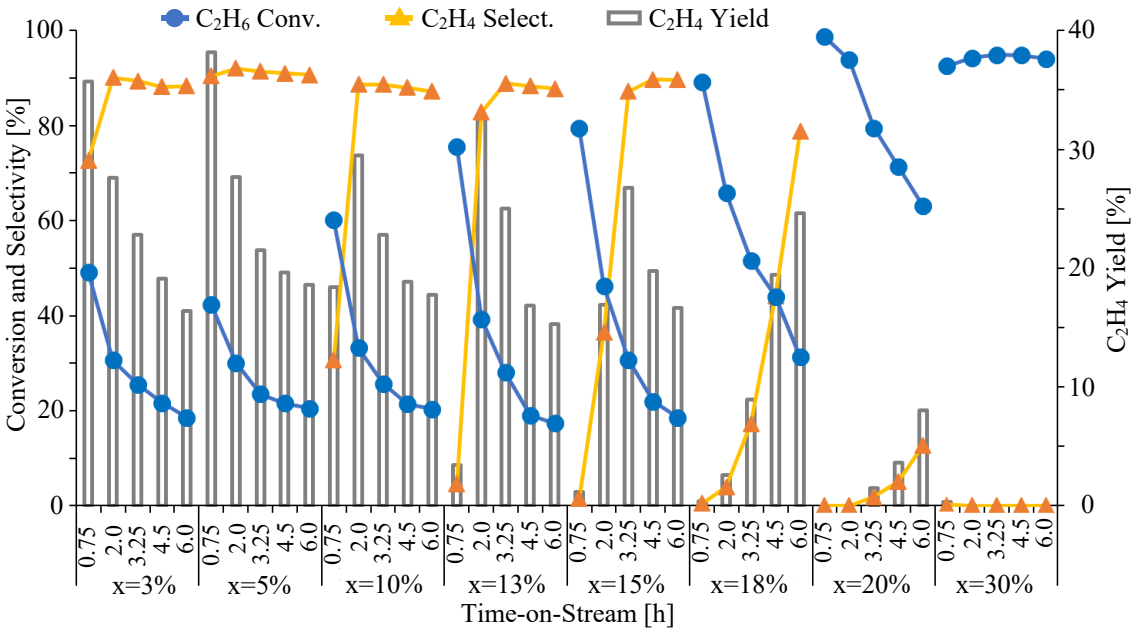

Fig. 1 The dehydrogenation of ethane at 923K on NiO(x)/γ-Al_2O_3

respectively) and selectivity to the product *i* (S*i*) were defined as follows:

C_{C2H6} (%) = 100 × [1-C_2H_6(P)/C_2H_6(R)]
C_{C3H8} (%) = 100 × [1-C_3H_8(P)/C_3H_8(R)]
S*i* (%) = 100 × [C*i*/(ΣC_1 + 2ΣC_2 + 3ΣC_3) for C_1 species
S*i* (%) = 100 × [2C*i*/(ΣC_1 + 2ΣC_2 + 3ΣC_3) for C_2 species
S*i* (%) = 100 × [3C*i*/(ΣC_1 + 2ΣC_2 + 3ΣC_3) for C_3 species

These equations were estimated using the absolute calibration method, where C_1, C_2, C_3, and C*i* refer to moles of C_1, C_2, C_3, and product *i,* respectively, in the product gas; C_2H_6(P) and C_2H_6(R) refer to moles of C_2H_6 in the product and reactant gas; and, C_3H_8(P) and C_3H_8(R) refer to moles of C_3H_8 in the product and reactant gas. The yields of ethylene and propylene were calculated from the product of the conversion of each reactant and the selectivity toward each product.

2. Results and Discussions

2.1 Catalytic performances

Figure 1 shows the catalytic performances for the dehydrogenation of ethane at 923 K on NiO(x)/γ-Al_2O_3. In this case, ethylene and methane were detected as products, and the production behavior of ethylene appears in Figure 1. On the NiO(x)/γ-Al_2O_3 (x = 3-10%) catalyst, the conversion of ethane and the yield of ethylene was decreased with time-on-stream, as observed in normal dehydrogenation reactions. However, on NiO(13)/γ-Al_2O_3 and NiO(15)/γ-Al_2O_3, the yield of ethylene was increased to 2.0 and 3.25 hours on-stream, respectively, and then decreased. Furthermore, when NiO(18)/γ-Al_2O_3 and NiO(20)/γ-Al_2O_3 were used, the yield of ethylene increased with time-on-stream and showed the same behavior as the catalytic dehydrogenation of isobutane (Sugiyama *et al.*, 2021). On the other hand, NiO(30)/γ-Al_2O_3 showed no activity. Generally, in a gas-solid heterogeneous catalyst system, the loading of the catalytic active species is several percentage points. As shown in Figure 1, with normal loading using this catalyst system, the catalyst deactivated normally. By changing isobutane to ethane as a reactant, however, the yield of the corresponding product was improved with time-on-stream with a specific loading of 18 to 20% in this catalyst system. Therefore, an improvement in the yield of isobutene with time-on-stream was observed, but improvement in the yield of ethylene was accomplished only at this specific level of loading.

Figure 2 shows the catalytic performances for the dehydrogenation of propane at 823 K on NiO(x)/γ-Al_2O_3. In this case as well, the deactivation behavior of the catalytic activity was similar to that of the dehydrogenation of ethane. When NiO(3)/γ-Al_2O_3 and NiO(5)/γ-Al_2O_3 were used, normal deactivation behavior was observed wherein the conversion of propane and the yield of propylene were drastically decreased with time-on-stream. On the other hand, when the loading of NiO was greater than that of NiO(15)/γ-Al_2O_3, the yield of propylene increased and the absolute value of the yield decreased with time-on-stream. On NiO(8)/γ-Al_2O_3 and NiO(10)/γ-Al_2O_3, which

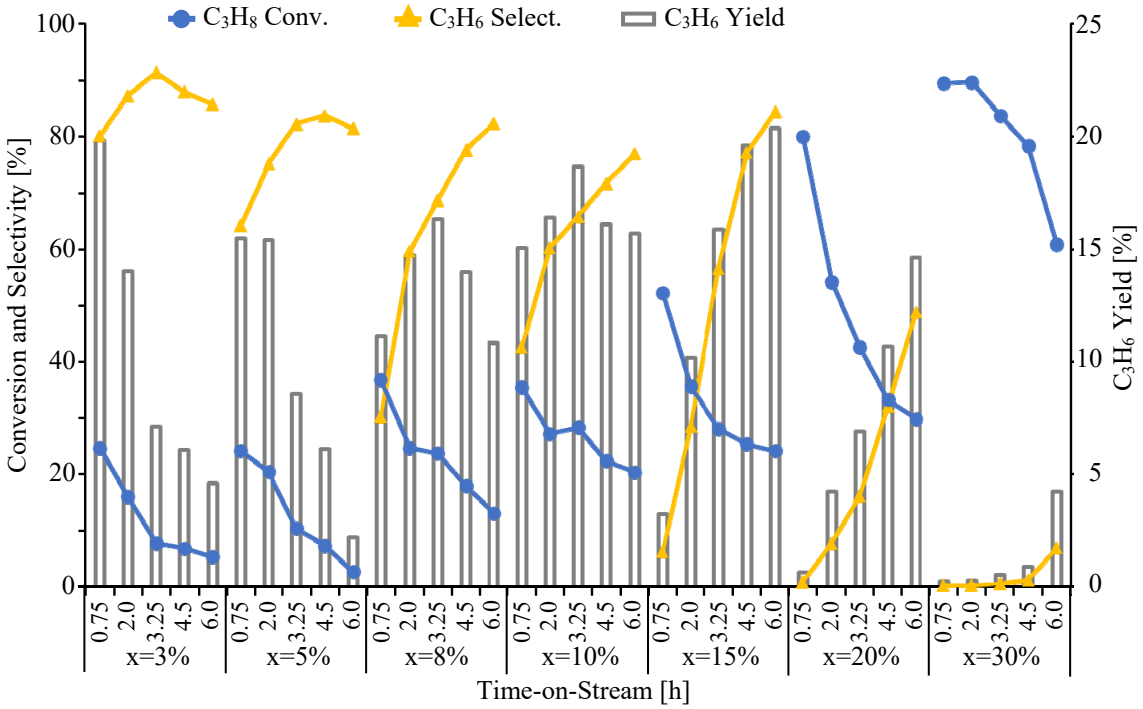

Fig. 2 The dehydrogenation of propane at 823 K on NiO(x)/γ-Al_2O_3

Table 1 Selectivity to by-product on NiO(x)/γ-Al_2O_3 corresponded to the results shown in Figure 2

TON*	By-product	x=3%	x=5%	x=8%	x=10%	x=15%	x=20%	x=30%
0.75 h	CH_4	9.5	14.2	60.6	49.7	93.8	94.0	99.7
	C_2H_4	10.3	13.2	9.1	5.1	0.0	0.0	0.0
2.0 h	CH_4	5.7	8.0	29.6	30.5	71.4	69.7	99.7
	C_2H_4	6.9	11.0	10.7	9.3	0.0	13.7	0.0
3.75 h	CH_4	3.5	5.4	20.1	24.7	43.5	59.3	99.4
	C_2H_4	5.0	7.9	11.1	9.5	6.5	16.2	0.0
4.5 h	CH_4	4.4	4.2	11.3	19.0	22.8	39.0	98.8
	C_2H_4	7.5	6.6	11.0	9.2	8.0	19.7	0.0
6.0 h	CH_4	5.2	4.5	7.9	13.3	15.6	25.6	93.1
	C_2H_4	9.0	7.4	9.8	9.7	8.5	17.3	0.0

* Time-on-stream

had an intermediate NiO loading in the present study, the yield of propylene showed the maximum value at 3.25 h on-stream, and an intermediate behavior between a catalyst with a lower loading of NiO and a catalyst with the higher loading of NiO was detected. These results confirmed that the time-on-stream increase in the yield of the alkene product observed in the dehydrogenation of isobutane on NiO/γ-Al_2O_3 was also observed in the dehydrogenations of both ethane and propane, although the loading of NiO varied depending on the respective reactant alkanes. In the dehydrogenation of propane, methane and ethylene were produced together with propylene. As shown in **Table 1**, when the NiO loading was low, that is, when the conversion of propane was low, methane and ethylene were obtained with similar selectivity. On the other hand, when the NiO loading increased and the conversion of propane increased, the selectivity to ethylene decreased sharply, and methane was the main by-product. In other words, it was clear that highly reactive ethylene directly contributed to carbon deposition, while stable methane did not contribute as much to carbon deposition.

Based on the results shown in Figures 1 and 2, the catalytic activity for the dehydrogenation of ethane on NiO(18)/γ-Al_2O_3 and that of propane on NiO(15)/γ-Al_2O_3 may be further improved with the extension of time-on-stream. Therefore, both dehydrogenations were examined over 12.0 h on-stream. **Figures 3 (A) and (B)** showed the catalytic activity for the dehydrogenation of ethane on NiO(18)/γ-Al_2O_3 and that of propane on NiO(15)/γ-Al_2O_3, respectively. The yield of ethylene reached maximum at 7.0 h on-stream, while that of propylene followed at 8.0 h on-stream. The behavior in which the yield of the dehydrogenation product was at maximum in a certain time-on-stream was similar to the dehydrogenation of isobutane using this catalytic system (Sugiyama *et al*., 2021). Since a longer period for time-on-stream results in the excess formation of carbon deposition over the catalyst surface, the expected improvement behavior of the activity with time-on-stream was not observed.

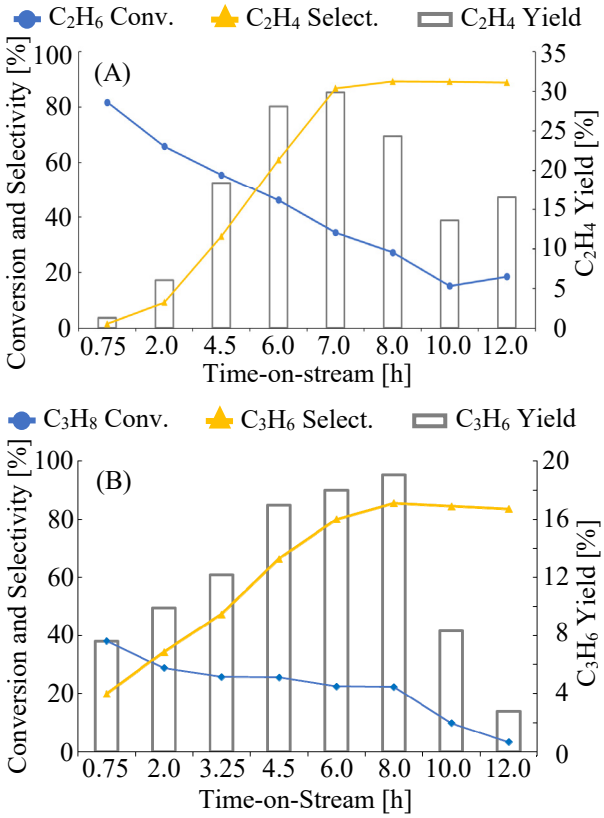

Fig. 3 The dehydrogenation of (A) ethane on NiO(18)/γ-Al_2O_3 at 923 K and that of (B) propane on NiO(15)/γ-Al_2O_3 at 823 K

2.2 Characterization of fresh catalysts

In order to obtain information on the structure of the fresh catalysts, XRD and nitrogen adsorption isotherm measurements were employed.

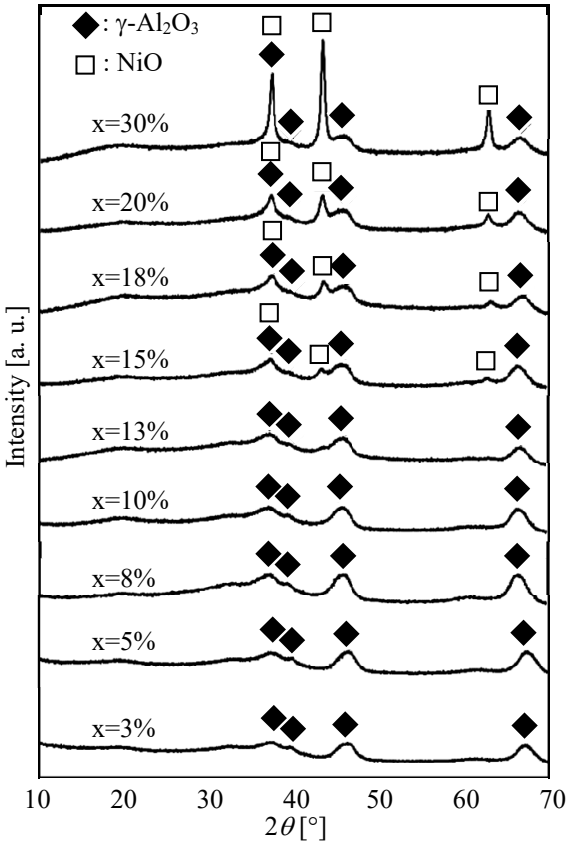

Fig. 4 XRD patterns of fresh NiO(x)/γ-Al_2O_3

Table 2 Specific surface areas, total pore volumes, and average pore diameters for the fresh NiO(x)/γ-Al_2O_3

NiO(x)/ γ-Al_2O_3	Specific surface area [m^2/g]	Total pore volume [cm^3/g]	Average pore diameter [nm]
x=3%	192	0.643	13.4
x=5%	199	0.668	13.4
x=8%	194	0.638	13.2
x=10%	193	0.600	12.4
x=13%	187	0.590	12.6
x=15%	182	0.552	12.1
x=18%	177	0.540	12.2
x=20%	156	0.519	13.3
x=30%	137	0.386	11.2

The XRD patterns of the fresh NiO(x)/γ-Al_2O_3 catalysts are shown in **Figure 4**. The XRD peaks due to γ-Al_2O_3 (PDF 00-010-0425; Prins, 2020) were detected from all the catalysts while the peaks due to NiO (PDF 03-065-6920) were also detected from NiO(x)/γ-Al_2O_3 at 15<x<30. Therefore, no formations were detected for oxide complexes consisting of γ-Al_2O_3 and NiO.

Table 2 shows the specific surface areas, total pore volumes, and average pore diameters for the fresh samples of NiO(x)/γ-Al_2O_3. The specific surface areas and total pore volumes were decreased with an increase in each loading except those from NiO(3)/γ-Al_2O_3, while the average pore diameters were rather insensitive to the NiO loading.

2.3 Characterization of previously used catalysts

To examine the carbon deposition and conversion from NiO to metallic Ni during the reaction, XRD and TGA for the catalysts used in the dehydrogenations of both ethane and propane were employed.

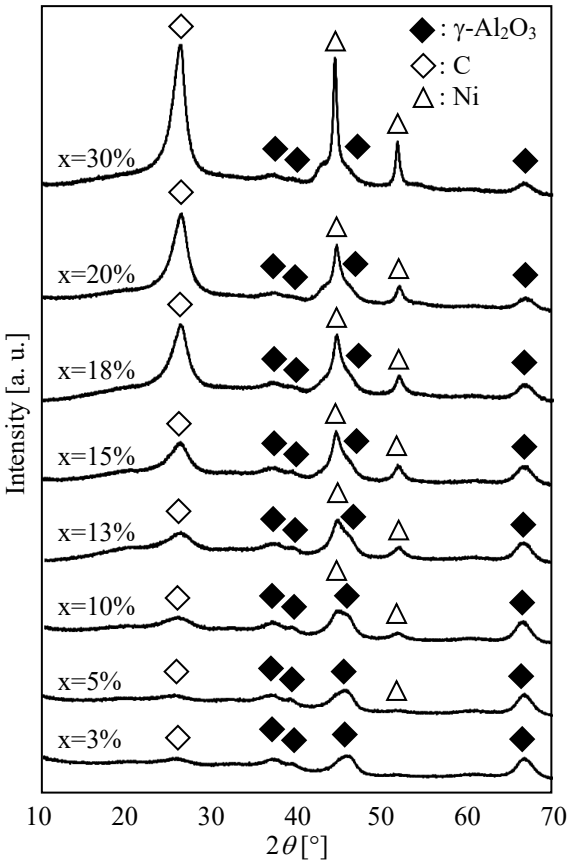

Fig. 5 XRD patterns of NiO(x)/γ-Al_2O_3 used in the dehydrogenation of ethane

Figure 5 shows the XRD of NiO(x)/γ-Al_2O_3 previously used to obtain the results shown in Figure 1 for the dehydrogenation of ethane. XRD signals due to carbon (PDF 01-082-9929) and γ-Al_2O_3 were detected regardless of the NiO loading. Among them, the intensity of the former signal was increased with NiO loading. XRD peaks due to metallic Ni (PDF 01-078-7533) were detected at a NiO loading greater than 5%, while the intensity of the Ni peaks increased with the NiO loading. Therefore, when the reduction of NiO to

metallic Ni occurred during the dehydrogenation of ethane, each catalyst was simultaneously covered with carbon mainly according to the level of NiO loading. Normally, when such a clear carbon deposition was investigated, the yield of the dehydrogenation product with time-on-stream was not improved. Therefore, when the results of Figures 1 and 5 are compared, the results are different from those of the normal catalytic reaction, particularly with NiO loadings of 18 and 20%.

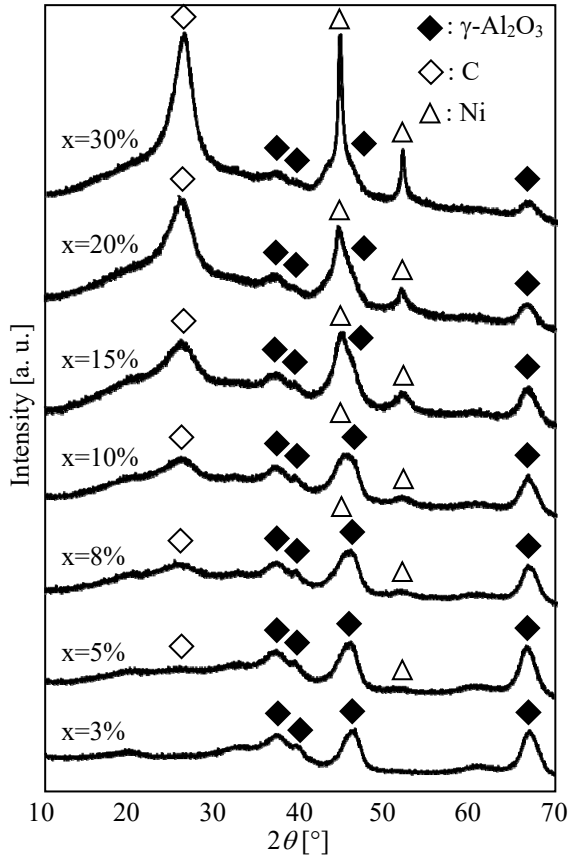

Fig. 6 XRD patterns of NiO(x)/γ-Al_2O_3 used in the dehydrogenation of propane

Figure 6 shows the XRD of NiO(x)/γ-Al_2O_3 that was previously used to obtain the results shown in Figure 2 for the dehydrogenation of propane. Since the reaction temperature of the catalytic activity test was performed at 100 K lower in Figure 6 than that in Figure 5, the XRD signals of all the catalysts became broader overall. However, as the NiO loading increased, the peaks associated with carbon deposition and the reduction of NiO to Ni became evident. As shown in Figures 5 and 6, metallic Ni was detected in NiO(x)/γ-Al_2O_3. However, it should be noted that the main peak due to metallic Ni appeared at around $2\theta = 44°$ in those figures, which matched the main peak due to Ni_3C (nickel carbide) (Uhlig *et al*., 2013). Furthermore, similar carbide species are known to be active sites for the dehydrogenation of n-butane (Neylon *et al*., 1999; Kwon *et al*., 2000), the dry reforming of methane and so on (Czaplicka *et al*., 2021). Since the reaction temperature was rather low for the formation of nickel carbide species (Czaplicka *et al*., 2021), it was assumed that metallic nickel was produced here. Based on the results shown in Figures 5 and 6, the formation of carbon deposition and the reduction of NiO to metallic Ni would contribute to an enhancement of the yield of propylene as in the dehydrogenation of isobutane to isobutene on NiO/γ-Al_2O_3 (Sugiyama *et al*., 2021).

The NiO/γ-Al_2O_3 catalyst used in the present study is known to be easily converted to the spinel structure of $NiAl_2O_4$ during various reactions (Shimoda *et al*., 2018, 2020). Once $NiAl_2O_4$ is produced, it is known that Ni^{2+} in this complex oxide is less likely to be reduced than Ni^{2+} in NiO. Under the present experimental conditions, the formation of $NiAl_2O_4$ could not be detected by XRD, and metallic nickel was detected even in the catalyst with a low loading of NiO. Therefore, it could be concluded that carbon deposition occurred around the nickel species from the beginning of the reaction, and this carbon deposition prevented the contact between the Ni species and γ-Al_2O_3, which was followed by a suppression of the formation of $NiAl_2O_4$.

Thermogravimetric analysis was performed to quantify the amount of carbon deposition as a factor for the improvement that was detected in the present study.

Table 3 The carbon deposition rate (CDR) for NiO(x)/γ-Al_2O_3 previously used to obtain the results shown in Figures 1 and 2 for the dehydrogenations of ethane and propane, respectively

NiO(x)/ γ-Al_2O_3	Reactant	CDR per 1g of NiO(x)/γ-Al_2O_3 [g/g]	CDR per 1g of NiO [g/g]
x=3%	Ethane	0.35	11.7
x=5%	Ethane	0.28	5.57
x=10%	Ethane	0.49	4.91
x=13%	Ethane	0.61	4.66
x=15%	Ethane	0.43	2.90
x=18%	Ethane	1.36	7.58
x=20%	Ethane	1.94	9.68
x=30%	Ethane	2.40	7.99
x=3%	Propylene	0.11	3.65
x=5%	Propylene	0.15	3.05
x=8%	Propylene	0.42	5.28
x=10%	Propylene	0.50	5.01
x=15%	Propylene	0.73	4.85
x=20%	Propylene	1.24	6.21
x=30%	Propylene	2.26	7.52

As shown in **Table 3**, both the carbon deposition rates (CDR) per 1g of NiO(x)/γ-Al_2O_3 and per 1 g of NiO were ineffective for the dehydrogenation of ethane and propane. Furthermore, both rates were not correlated to the NiO loading. In either form of

dehydrogenation, however, when x=3% or x=5%, the carbon deposition rates per 1 g of NiO(x)/γ-Al_2O_3 were small, and in this case, the yield of the dehydrogenation product was decreased with time-on-stream, as shown in Figures 1 and 2. In addition, both dehydrogenations showed almost no activity when the carbon deposition rates per 1 g of NiO(x)/γ-Al_2O_3 or NiO were as large as x=30%. This result indicates that when the amount of the carbon deposition is small, normal deactivation behavior is observed, but when the amount of the carbon deposition is too large, no activity is detected.

Figures 7 (A) and **(B)** showed the thermogravimetric curve (TG curve) of NiO(x)/γ-Al_2O_3 previously used to obtain the results shown in Table 3 for the dehydrogenations of ethane and propane, respectively. The use of either ethane or propane as a reactant allowed us to estimate whether the carbon deposition produced was a similar species or a completely different species base on the temperature at which the weight reduction began.

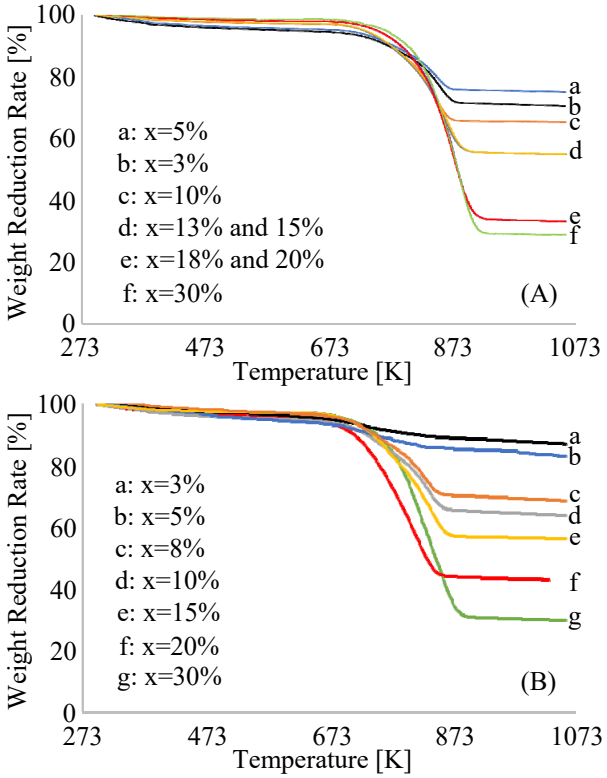

Fig. 7 TG curves of NiO(x)/γ-Al_2O_3 used in the dehydrogenation of (A) ethane and (B) propane

As shown in Figure 7 (A), when using NiO(x)/γ-Al_2O_3 for the dehydrogenation of ethane, TG curves from NiO(13)/γ-Al_2O_3 and NiO(15)/γ-Al_2O_3 together with those from NiO(18)/γ-Al_2O_3 and NiO(20)/γ-Al_2O_3 were overlapped on almost the same curve. The weight reduction rates were on the order of the NiO loading except for NiO loadings of 3% and 5%, and the temperature at which the weight reduction occurred was observed in the same temperature range regardless of the NiO loading. When NiO(x)/γ-Al_2O_3 was previously used for the dehydrogenation of propane (Figure 7 (B)), the weight reduction rate was in the order of the NiO loading, and the temperature at which the weight reduction occurred was in the same range as that of ethane, regardless of the NiO loading. These results indicate that the carbon depositions formed after both dehydrogenations show similar properties regardless of whether the reactant is ethane or propane, at least based on the results of the TG analysis.

FE-SEM measurements were performed to examine the status of carbon deposition using the catalysts previously employed in obtaining the results shown in Figures 1 and 2. For the measurement samples, NiO(5)/γ-Al_2O_3 was selected as the catalyst, which showed normal deactivation behavior in the dehydrogenations of both ethane and propane. Furthermore, NiO(18)/γ-Al_2O_3 and NiO(20)/γ-Al_2O_3 were also selected because these showed an increase in the yield of the target product with time-on-stream in the dehydrogenations of ethane and propane, respectively. As shown in **Figure 8**, the catalyst surfaces after the reaction differed considerably depending on the reactant and the NiO loading. It should be noted that when the yield of the target product was increased with time-on-stream, fine fibrous substances were detected on the catalyst surfaces, as shown in **Figures 8 (B)** and **(D)**. These fine fibrous substances were considered to correspond to the carbon deposition discussed above. In contrast, the fibrous substances are not detected in **Figures 8 (A)** and **(C)**, both of which showed normal deactivation behavior.

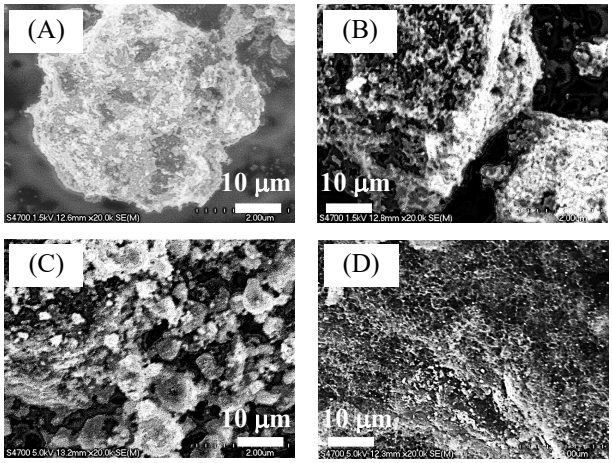

Fig. 8 FE-SEM images of (A) NiO(5)/γ-Al_2O_3 and (B) NiO(18)/γ-Al_2O_3 used to obtain the results shown in Figure 1 and (C) NiO(5)/γ-Al_2O_3 and (D) NiO(20)/γ-Al_2O_3 used to obtain the results shown in Figure 2

Therefore, it was confirmed that carbon deposition similar to nanotube-like carbon deposition detected after the dehydrogenation of isobutane on NiO/γ-Al_2O_3 was

also formed in the dehydrogenations of both ethane and propane. From these results, it can be concluded that, as with the dehydrogenation of isobutane on NiO/γ-Al_2O_3 (Sugiyama *et al*., 2021), the high dispersion of Ni metal associated with such fibrous carbon deposition led to an improvement in the yield of the target product when using both ethane and propane as a reactant in the special loading of NiO. In the dehydrogenations of both ethane and propane on NiO/γ-Al_2O_3, when the NiO loading was less than 5%, there was no fibrous carbon deposition. Therefore, normal catalyst deactivation behavior was observed. On the other hand, when the NiO loading was as high as 30%, the Ni metal highly dispersed on fibrous carbon was further covered with carbon, which resulted in a disappearance of catalytic activity.

Raman spectroscopy of NiO(18)/γ-Al_2O_3 and NiO(20)/γ-Al_2O_3 was used to obtain the results shown in Figure 1 for the dehydrogenation of ethane and in Figure 2 for that of propane, respectively, to investigate the effects of different reaction substrates on the properties of carbon deposition. Raman spectroscopy of carbon nanotubes consisting of graphene (Iijima and Ichihashi, 1993) has shown three types of signals (Ferrari *et al*., 2006; Dresselhaus *et al*., 2010; Wang *et al*., 2019; Piao *et al*., 2021). The signals appearing around 2,700; 1,580; and, 1,350 cm^{-1} in the Raman shift are due to the crystallinity of graphite, the planar structure of graphite, and the defective structure of graphite. And they are referred to as the G'-band, G-band, and D-band, respectively. A smaller intensity ratio for the G-band and D-band signals (G/D ratio) translates to a lack of progress in the crystallization of carbon nanotubes.

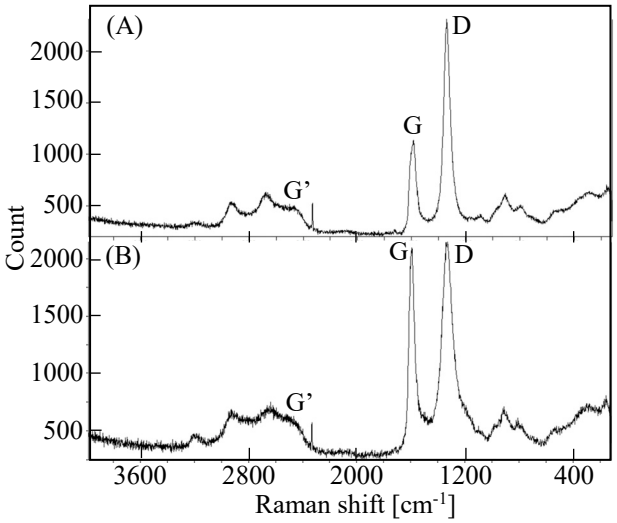

Fig. 9 Raman spectra of (A) NiO(18)/γ-Al_2O_3 and (B) NiO(20)/γ-Al_2O_3 previously used for obtaining results shown in Figure 1 for the dehydrogenation of ethane and Figure 2 for that of propane, respectively.

Figures 9 (A) and **(B)** show the Raman spectra of NiO(18)/γ-Al_2O_3 and NiO(20)/α-Al_2O_3 recovered after obtaining the results shown in Figures 1 and 2, respectively. Slight signals due to the G'-band were detected, regardless of whether the use was for the dehydrogenation of ethane or propane. The most notable difference was that the intensity of the signal derived from the G-band was smaller in NiO(18)/γ-Al_2O_3 used for ethane dehydrogenation (Figure 9 (A)) than in NiO(20)/α-Al_2O_3 used for propane dehydrogenation (Figure 9 (B)). As a result, the intensity of the G/D ratio obtained from Figure 9 (A) (0.43) was clearly smaller than the value obtained from Figure 9 (B) (0.98). This indicates that the crystallization has not progressed on NiO(18)/γ-Al_2O_3 used for ethane dehydrogenation as compared with NiO(20)/α-Al_2O_3 used for propane dehydrogenation. Therefore, it was confirmed that the influence of the reaction substrate determines on the crystallinity of the carbon deposition.

2.4 Comparison of dehydrogenation activity of ethane, propane, and isobutane on NiO(20)/γ-Al_2O_3 under the same conditions

In this catalyst system, in order to compare the activity behavior with time-on-stream when the reaction substrates are ethane, propane and isobutane, the comparison was performed on 0.25 g of NiO(20)/γ-Al_2O_3 with the reaction temperature at 823 K, the partial pressure of each alkane at 14.1 kPa, and at a total flow rate at 15 mL/min.

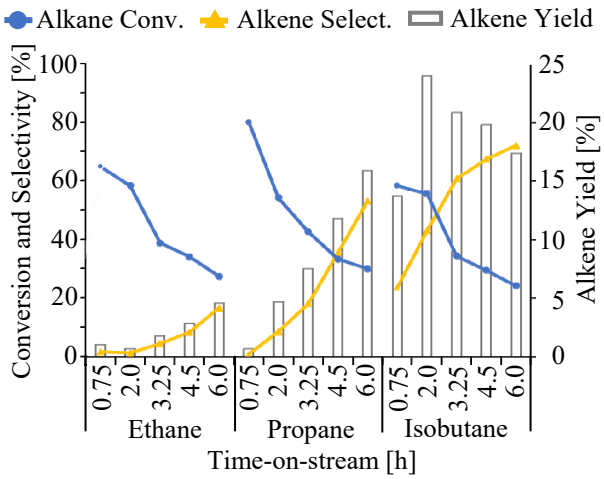

Fig. 10 The dehydrogenation of ethane, propane, and isobutane at 823 K on NiO(20)/γ-Al_2O_3

As shown in **Figure 10**, the dehydrogenations of ethane and propane were improved with time-on-stream, resulting in the enhancement of the yield and selectivity to each dehydrogenated product with time-on-stream. As expected, the dehydrogenation activity for propane was higher than that for ethane. On the other hand, with isobutane dehydrogenation, the yield

and selectivity to isobutene were improved up to 2.0 h on-stream, while the yield of isobutene reached maximum at 2.0 h on-stream, and then decreased with time-on-stream. The carbon deposition rates (CDR) per 1g of NiO(20)/γ-Al_2O_3 previously used for the dehydrogenation of ethane, propane, and isobutane at 2.0 h on-stream were 0.66, 1.24, and 2.53, respectively. As previously reported (Sugiyama *et al.*, 2021), the reaction temperature of 823 K was too high for the dehydrogenation of isobutane, resulting in the formation of an excess amount of carbon deposition over the catalyst surface. Since this carbon deposition could cover the catalytically active Ni species after 2.0 h on-stream, the activity has decreased after 2.0 h on-stream.

2.5 Reduction of NiO to metallic Ni at initial time-on-stream

As shown in Figures 5 and 6, nickel oxide in NiO(x)/γ-Al_2O_3 was reduced to metallic nickel after dehydrogenation at 6.0 h on-stream. It has been reported that nickel oxide supported on γ-alumina is reduced to metallic nickel when using hydrogen at temperatures lower than 673 K (Heracleous *et al.*, 2005). In addition, our laboratory also revealed that only metallic nickel signal was detected from the XRD of NiO(20)/γ-Al_2O_3 recovered after the dehydrogenation of isobutane at 0.1 h on-stream (Sugiyama *et al.*, 2022). Therefore, in the present reaction systems as well, the reduction of NiO to metallic Ni is expected to proceed in the early stages of each dehydrogenation. Therefore, the activity of the metallic Ni may also be reflected in the activity at 0.5 h on-stream, and longer, in Figures 1 and 2.

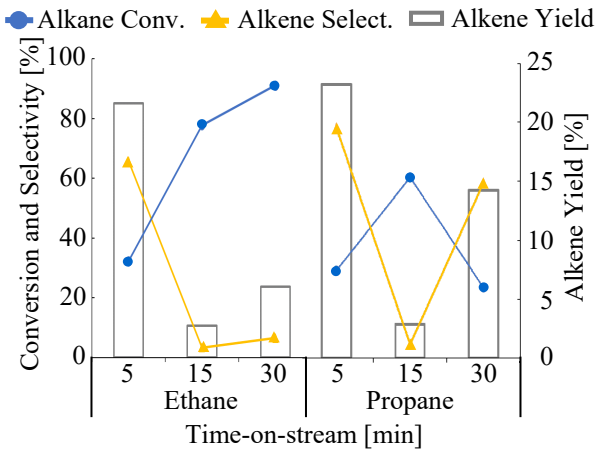

Fig. 11 Initial activity for the dehydrogenation of ethane on NiO(18)/γ-Al_2O_3 at 923 K and propane on NiO(15)/γ-Al_2O_3 at 823 K

To confirm this prediction, the dehydrogenation of ethane on NiO(18)/γ-Al_2O_3 at 923 K and that of propane on NiO(15)/γ-Al_2O_3 at 823 K were examined at 5, 15, and 30 min on-stream, respectively, and the XRD of the catalysts recovered after these short periods of time-on-stream were measured. **Figure 11** shows the initial activity until 30 min on-stream for the dehydrogenation of ethane on NiO(18)/γ-Al_2O_3 at 923 K and that on NiO(15)/γ-Al_2O_3 at 823 K, in which both catalysts were prepared separately and different from those used in Figures 1 and 2. For both systems, the great yield at 5 min on-stream was decreased at 15 min on-stream, followed by an increase at 30 min on-stream. This indicated that both systems demonstrated catalytic activity at 5 min on-stream that reflects the nature of NiO, while that at time-on-stream longer than 15 min reflects the nature of metallic Ni. This can be further supported by the XRD of the catalysts previously used in obtaining the results shown in Figure 11.

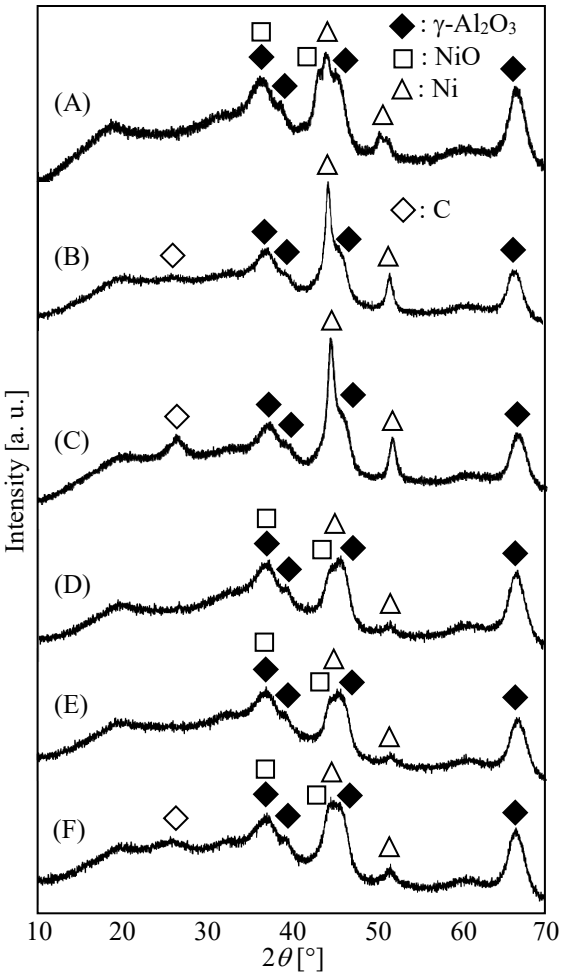

Fig. 12 XRD patterns of NiO(18)/γ-Al_2O_3 used in the dehydrogenation of ethane at (A) 5, (B) 15, and (C) 30 min on-stream and those of NiO(15)/γ-Al_2O_3 used in the dehydrogenation of propane at (D) 5, (E) 15, and (F) 30 min on-stream.

Figure 12 shows the XRD patterns of NiO(18)/γ-Al_2O_3 and NiO(15)/γ-Al_2O_3 used for obtaining the results shown in Figure 11, respectively. XRD patterns

of NiO(18)/γ-Al_2O_3 used for the dehydrogenation of ethane at 5 min on-stream (Figure 12 (A)) showed the presence of metallic Ni with NiO, while the peaks due to metallic Ni were not detected at 15 min on-stream (Figure 12 (B)) and longer (Figure 12 (C)). At 5 min on-stream, the presence of NiO seemed to contribute to great activity for dehydrogenation (Figure 11), since it was previously reported that oxide catalysts such as NiO (Ding *et al*., 2010b) and Cr_2O_3 (Grzybowska *et al.*, 1998) showed high activity for dehydrogenation. After 15 min on-stream, metallic Ni but not NiO was detected, but it is expected that this metallic Ni was present on the support at a lower dispersion and not present on the carbon nanotubes, which resulted in lower activity. At 30 min on-stream, metallic Ni may highly disperse with time-on-stream on the carbon deposition detected in Figure 12 (C), which resulted in the enhancement of the activity at 30 min on-stream and longer. In the case of NiO(15)/γ-Al_2O_3 used for the dehydrogenation of propane, XRD signals were broader than those in NiO(18)/γ-Al_2O_3 in the dehydrogenation of ethane, since the reaction temperature for propane dehydrogenation was 100 K lower than that for ethane dehydrogenation. Therefore, it was clarified that the reduction of NiO to metallic Ni was slower in the NiO(15)/γ-Al_2O_3 used for the dehydrogenation of propane (Figures 12 (D) – (F)) than in NiO(18)/γ-Al_2O_3 when used for the dehydrogenation of ethane (Figures 12 (A) – (C)), but this reduction proceeded in the early stages of time-on-stream for both dehydrogenations. It is also clear that the formation of carbon deposition was slower with NiO(15)/γ-Al_2O_3, as shown in Figure 12 (F). These results indicate that the metallic Ni converted from NiO formed on carbon deposition contributes to the improvement of the catalytic activity for the dehydrogenations of both ethane and propane.

Conclusions

In our previous report, we described how the yield of the target product increased with time-on-stream in the dehydrogenation of isobutane on NiO/γ-Al_2O_3. It was confirmed that the same behavior was exhibited with a specific level of NiO loading even in the dehydrogenations of both ethane and propane when using the same catalyst. In normal catalytic dehydrogenations, the yield of the target product decreases sharply with time-on-stream. Therefore, this behavior was completely different from the conventional results. The results of this study, however, confirmed the phenomenon whereby the yield of the target product increases with time-on-stream even in the dehydrogenations of both ethane and propane on the same catalyst, NiO/γ-Al_2O_3, although the Ni loading was specific. Even in the case for the dehydrogenations of ethane, propane and isobutane, the yields of the target product were not improved with time-on-stream unless the NiO loading was smaller than 15%. Therefore, it was concluded that such behavior could not be observed in the catalytic reaction using the supported nickel catalyst with a loading of several percentage points. We suggest that when Ni metal forms with a high degree of dispersion on fibrous carbon deposition during dehydrogenation, this contributes to an improvement in the yield of the target product with time-on-stream.

Acknowledgements

This study was supported by JSPS KAKENHI Grant Number JP20K05221, for which we are grateful. The authors gratefully acknowledge Mr. Tomoyuki Ueki of Graduate School of Technology, Industrial and Social Science, Tokushima University for his help and valuable suggestions in the Raman spectroscopy.

Literature Cited

Alvarez-Galvan C., M. Melian, L. Ruiz-Matas, J. L. Eslava, R. M. Navarro, M. Ahmadi, B. R. Cuenya and J. L. G. Fierro; "Partial Oxidation of Methane to Syngas over Nickel-Based Catalysts: Influence of Support Type, Addition of Rhodium, and Preparation Method," *Front. Chem*., **7**:104, doi: 10.3389/fchem.2019.00104 (2019)

Argyle, M. D. and C. H. Bartholomew; "Heterogeneous Catalyst Deactivation and Regeneration: A Review," *Catalysts*, **5**, 145-269 (2015)

Arora, S. and R. Prasad; "An Overview on Dry Reforming of Methane: Strategies to reduce carbonaceous deactivation of Catalysts," RSC Adv., 6, 108668-108688 (2016)

Avevalo, R. L., S. M. Aspera, M. C. S. Escaño, H. Nakanishi and H. Kasai; "Tuning Methane Decomposition on Stepped Ni Surface," *Sci. Reports*, **7**, 13963 (2017)

Besenbacher, F., I. Chorkendorff, B. S. Clausen, B. Hammer, A. M. Molenbroek, J. K. Nørskov and I. Stensgaard; "Design of a Surface Alloy Catalyst for Steam Reforming," *Science*, **279**, 1913-1915 (1998)

Bradford, M. C. J. and M. A. Vannice; "The Roel of Metal-Support Interaction in CO_2 Reforming of CH_4," *Catal. Today*, **50**, 87-96 (1999)

Czaplicka, N., A. Rogala and I. Wysocka; "Metal (Mo, W, Ti) Carbide catalysts: Synthesis and Application as Alternative catalysts for Dry Reforming of Hydrocarbons – A Review," *Int. J. Mol. Sci.*, **22**, 12337 (2021)

Ding, J., R. Shao, J. Wu, Z. Qin and J. Wang; "Coupling Dehydrogenation of Isobutane to Produce Isobutene in Carbon Dioxide over NiO/γ-Al_2O_3 Catalyst," *React. Kinet. Mech. Catal*., **101**, 173–181 (2010a)

Ding, J., Z. Qin, X. Li, G. Wang and J. Wang; "Catalytic Dehydrogenation of isobutane in the presence of Carbon Dioxide over Nickel Supported on Active Carbon," *J. Mol. Catal. A; Chem.*, **315**, 221-225 (2010b)

Dresselhaus, M. S., A. Jorio, M. Hofmann, G. Dresselhaus and R. Saito; "Perspectives on Carbon Nanotubes and Graphene Raman Spectroscopy," *Nano. Lett.*, **10**, 751-758 (2010)

Ferrari, A. C., J. C. Meyer, V. Scardaci, C. Casiraghi, M. Lazzeri, F. Mauri, S. Piscanec, D. Jiang, K. S. Novoselov, S. Roth and A. K. Geim; "Raman Spectrum of Graphene and Graphene Layers," *Phys. Rev. Lett.*, **97**, 187401 (2006)

Grzybowska, B., J. Słoczyński, R. Grabowski, K. Wcislo, A. Kozłowska, J. Stoch and J. Zieliński; "Chromium Oxide/Alumina Catalysts in Oxidative Dehydrogenation of Isobutane," *J. Catal*., **178**, 687-700 (1998)

Guo, Y., T. P. Tran, L. Zhou, Q. Zhang and H. Kameyama; "Steam Methane Reforming Using an Anodic Alumina Supported Nickel Catalyst (Ni/Al_2O_3/Alloy): Analysis of Catalyst Deactivation," *J. Chem. Eng. Japan*, **40**, 1221-1228 (2007)

Hayakawa, T., S. Suzuki, J. Nakamura, T. Uchijima, S. Hamakawa, K. Suzuki, T. Shishido and K. Takehira; "CO_2 Reforming of CH_4 over Ni/perovskite catalysts Prepared by Solid Phase Crystallization Method," *Appl. Catal. A. Gen.*, **183**, 273-285 (1999)

Heracleous, E., A. F. Lee, K. Wilson, and A. A. Lemonidou; "Investigation of Ni-Based Alumina-Supported Catalysts for the Oxidative Dehydrogenation of Ethane to Etylene: Structural Characterization and Reactivity Studies," *J. Catal*., **231**, 159-171 (2005)

Iijima, S. and T. Ichihashi; "Single-shell Carbon nanotubes of 1-nm diameter," *Nature*, **363**, 603-605

Kwon, H., L. T. Thompson, J. Eng, Jr. and J. G. Chen; "n-Butane Dehydrogenation over Vanadium Carbides: Correlating catalytic and Electronic Properties," *J. Catal*., **190**, 60–68 (2000)

Miura, Y., T. Uchijima and S. Makishima; "Effects of Iron and Nickel Catalysts on Carbon Precipitation and Tungsten Carbonization with Hydrocarbon Gases," *Kogyō Kagaku Zzassi* (*J. Chem. Ind.*) **71**, 86-92 (1968)

Neylon, M. K., S. Choi, H. Kwon, K. E. Kurry and L. T. Thompson; "Catalytic Properties of Early Trensition Metal Nitrides and Carbides: n-Butane Hydrogenolysis, Dehydrogenation and Isomerization," *Appl. Catal. A; Gen,* **183**, 253–263 (1999)

Ochoa, A., B. Aramburu, B. Valle, D. E. Resasco, J. Bilbao, A. G. Gayubo and P. Castaño; "Role of Oxygenates and Effect of Operating Conditions in the Deactivation of a Ni Supported Catalyst during the Steam Reforming of Bio-Oil," *Green Chem*., **19**, 4315-4333 (2017)

Otsuka, K. and S. Takenaka; "Synthesis of Pure Hydrogen through the Catalytic Decomposition of Methane," *Catal. (Shokubai)*, **45**, 298-300 (2003)

Piao, Y., V. N. Tondare, C. S. Davis, J. M. Gorham, E. J. Petersen, J. W. Gilman, K. Scott, A. E. Vladár and A. R. H. Walker; "Comparative Study of Multiwall Carbon Nanotube Nanocomposites by Raman, SEM, and XPS Measurement techniques," *Compos. Sci. Tech*., **208** 108753 (2021)

Prins, R.; "On the Structure of γ-Al_2O_3," *J. Catal*., **392**, 336-346 (2020)

Sehested, J.; "Four Challenges for Nickel Steam-Reforming Catalysts," *Catal. Today*, **111**, 103-110 (2006)

Shimoda, N., N. Koide, M. Kasahara, T. Mukoyama, and S. Satokawa; "Development of Oxide-Supported Nickel-Based Catalysts for Catalytic Decomposition of Dimethyl Sulfide," *Fuel*, **232**, 485-494 (2018)

Shimoda, N., N. Koide, T. Honma, T. Nakano, J. Zhang, H. Wakita, and S. Satokawa; "Local Structure Analysis of Active Sites in NiO/γ-Al_2O_3 Catalyst for Dimethyl Sulfide Decomposition: Sulfurization Behavior of Ni Species Using X-ray Absorption Spectroscopy Analysis," *J. Jpn. Petrol. Inst*., **63**, 365-374 (2020)

Sugiyama, S., K. Oribe, S. Endo, T. Yoshida, N. Shimoda, M. Katoh, Y. Kato, and W. Ninomiya; "Enhancement of the Catalytic Activity Associated with Carbon Deposition Formed on NiO/γ-Al_2O_3 Catalysts during the Direct Dehydrogenation of Isobutane," *J. Chem. Eng. Japan*, **54**, 35-43 (2021)

Sugiyama, S., T. Yoshida, N. Shimoda, T. Ueki, Y. Kato, and W. Ninomiya; "Carbon Deposition Assisting the Enhancement of Catalytic Activity with Time-on-Stream in the Dehydrogenation of Isobutane on NiO/Al_2O_3," *J. Chem. Eng. Japan*, submitted (2022)

Takehira, K., T. Shishido and M. Kondo; "Partial Oxidation of CH_4 over Ni/$SrTiO_3$ Catalysts Prepared bu a Solid-Phase Crystallization Method," *J. Catal*., **207**, 307-316 (2002)

Uhlig, S., R. Struis, H. Schmid-Engel, J. Bock, A.-C. Probst, O. Freitag-Weber, I. Zizak, R. Chernikov and G. Schultes; "Piezoresistive Ni:a-C:H Thin Films Containing hcp-Ni or Ni_3C Investigated by XRD, EXAFS, and Wavelet Analysis," *Diam. Relat. Mater.*, **34**, 25–35 (2013)

Ye, G., H. Wang, X. Duan, Z. Sui, X. Zhou, M.-O. Coppens and W. Yuan; "Pore Network Modeling of Catalyst Deactivation By Coking, from Single Site to Particle, During Propane Dehydrogenation," *AIChE J*., **65**, 140-150 (2019)

Wang, W., C. Wang, X. Yue, C. Zhang, C. Zhou, W. Wu and H. Zhu; "Raman Spectroscopy and Resistance-Temperature Studies of Functionalized Multiwalled Carbon Nanotubes/epoxy Resin Composite Film," *Microelect. Eng*., **214**, 50-54 (2019)